Increased expression of BubR1 protects against aneuploidy and cancer and extends healthy lifespan

Darren J. Baker[1,2,6], Meelad M. Dawlaty[2,6], Tobias Wijshake[1,3], Karthik B. Jeganathan[1], Liviu Malureanu[1,2], Janine H. van Ree[1], Ruben Crespo-Diaz[4], Santiago Reyes[4], Lauren Seaburg[5], Virginia Shapiro[5], Atta Behfar[4], Andre Terzic[4], Bart van de Sluis[3] and Jan M. van Deursen[1,2,7]

The *BubR1* gene encodes for a mitotic regulator that ensures accurate segregation of chromosomes through its role in the mitotic checkpoint and the establishment of proper microtubule–kinetochore attachments. Germline mutations that reduce BubR1 abundance cause aneuploidy, shorten lifespan and induce premature ageing phenotypes and cancer in both humans and mice. A reduced BubR1 expression level is also a feature of chronological ageing, but whether this age-related decline has biological consequences is unknown. Using a transgenic approach in mice, we show that sustained high-level expression of BubR1 preserves genomic integrity and reduces tumorigenesis, even in the presence of genetic alterations that strongly promote aneuplodization and cancer, such as oncogenic Ras. We find that BubR1 overabundance exerts its protective effect by correcting mitotic checkpoint impairment and microtubule–kinetochore attachment defects. Furthermore, sustained high-level expression of BubR1 extends lifespan and delays age-related deterioration and aneuploidy in several tissues. Collectively, these data uncover a generalized function for BubR1 in counteracting defects that cause whole-chromosome instability and suggest that modulating BubR1 provides a unique opportunity to extend healthy lifespan.

During mitosis, duplicated chromosomes need to be separated equally amongst two identical cells. To ensure that this process occurs without errors, mammalian cells have developed a surveillance mechanism, the mitotic checkpoint, which inhibits anaphase onset until chromosome bi-orientation has been achieved. BubR1 is a core mitotic checkpoint component that binds to and inhibits the Cdc20-activated anaphase-promoting complex (APC/C^{Cdc20}), a ubiquitin E3 ligase that initiates anaphase by orchestrating separase-mediated cleavage of

cohesion rings that hold sister chromatids together[1]. BubR1 contributes to proper chromosome segregation not only through mitotic checkpoint activation but also by regulation of chromosome–spindle attachments[2,3]. Mutant mice carrying *BubR1* hypomorphic alleles (*BubR1*$^{H/H}$ mice) that produce low amounts of the protein are prone to aneuploidy and develop various progeroid and age-related phenotypes, including short lifespan, growth retardation, cataracts, sarcopenia, subdermal fat loss, impaired wound healing and reduced dermal thickness[1,4–6]. Mutations in BubR1 have been associated with mosaic variegated aneuploidy, a rare human syndrome characterized by aneuploidization, tumour predisposition and several progeroid traits, including short lifespan, growth and mental retardation, cataracts and facial dysmorphisms[7–9]. These data, together with the observation that BubR1 abundance declines with age in various mouse tissues[1,4,5], led to the notion that BubR1 may contribute to chronological ageing.

We reasoned that if depletion of BubR1 with age contributes to ageing and age-related disorders, then increased expression of BubR1 might extend healthy lifespan. To test this hypothesis, we generated transgenic mice expressing BubR1 fused to a Flag tag under the control of the ubiquitous CAGGS promoter (Fig. 1a). As a marker for transgene expression, we co-expressed enhanced green fluorescent protein (EGFP) from an internal ribosome entry site. Two independent BubR1 transgenic lines were obtained, henceforth referred to as T7 and T23. Western blot analysis of a broad spectrum of tissues indicated that T7 and T23 mice expressed moderate and high amounts of Flag–BubR1, respectively (Fig. 1b and Supplementary Fig. S1a–c). Expression of Flag–BubR1 corrected all premature ageing phenotypes of *BubR1*$^{H/H}$ mice (Fig. 1c, and data not shown), confirming that the Flag–BubR1 protein was functional and adequately expressed.

Key mitotic regulators such as Bub1, Mad2 and UbcH10 cause aneuploidy and tumour formation when overexpressed in mice[10–12]. However, T7 and T23 splenocytes and mouse embryonic fibroblasts

[1]Department of Pediatric and Adolescent Medicine, Mayo Clinic, 200 First Street Southwest, Rochester, Minnesota 55905, USA. [2]Department of Biochemistry and Molecular Biology, Mayo Clinic, 200 First Street Southwest, Rochester, Minnesota 55905, USA. [3]Department of Pathology and Medical Biology, University of Groningen, University Medical Center Groningen, Groningen 9700 RB, The Netherlands. [4]Department of Medicine, Mayo Clinic, 200 First Street Southwest, Rochester, Minnesota 55905, USA. [5]Department of Immunology, Mayo Clinic, 200 First Street Southwest, Rochester, Minnesota 55905, USA. [6]Joint first authors.
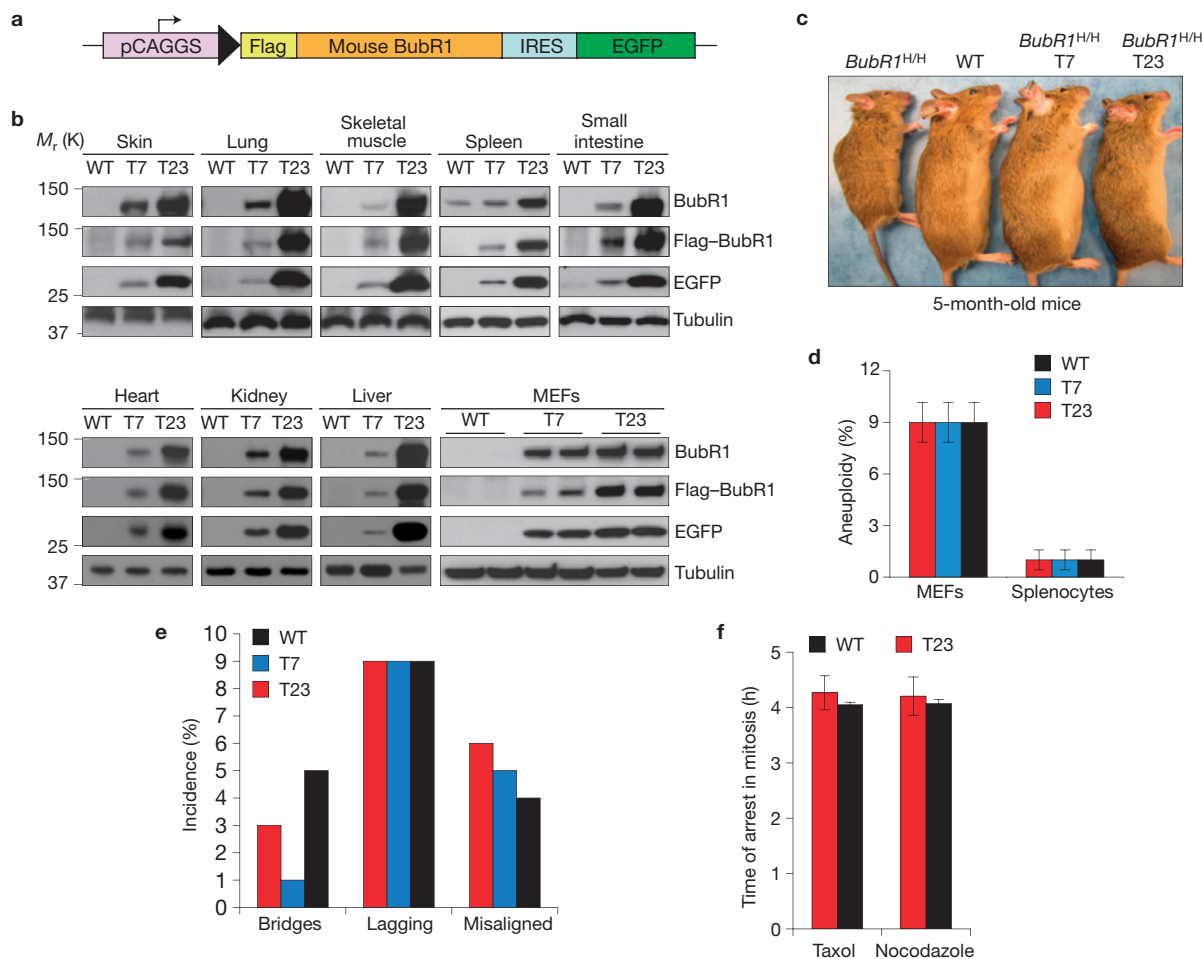[7]Correspondence should be addressed to J.M.v.D. (e-mail: vandeursen.jan@mayo.edu)

Figure 1 Transgenic mouse strains with moderate and high levels of Flag–BubR1 are chromosomally stable. (**a**) Flag–mBubR1 transgenic vector design. pCAGGS, promoter consisting of the CMV immediate enhancer and the chicken β-actin promoter; IRES, internal ribosome entry site. (**b**) Western blots of tissue and MEF extracts from wild-type (WT) and Flag–BubR1 transgenic mice (strains T7 and T23). Tubulin was used as a loading control. (**c**) Both Flag–BubR1 transgenes correct the growth retardation and ageing-associated phenotypes of $BubR1^{H/H}$ mice. (**d**) A high level of BubR1 expression does not induce aneuploidy. Chromosome counts were done on splenocytes from 5-month-old mice and P5 MEFs ($n = 3$ samples per genotype). Fifty spreads were counted per sample (150 total). Values represent means ± s.d. (**e**) High BubR1 levels do not induce chromosome missegregation. (**f**) The mitotic checkpoint is not hyperactive at supranormal BubR1 levels. Values represent means ± s.d. Three independent MEF lines per genotype were used in **e**,**f**. Uncropped images of blots are shown in Supplementary Fig. S6.

(MEFs) showed normal aneuploidy rates (Fig. 1d). Consistent with this, chromosome missegregation rates were not elevated in T7 and T23 MEFs (Fig. 1e). Transgenic MEFs showed increased BubR1–Cdc20 complex formation (Supplementary Fig. S1d), but this had no overt impact on mitotic checkpoint activity (Fig. 1f). Key mitotic regulators were expressed at normal levels in T23 MEFs (Supplementary Fig. S1e).

Tumour susceptibility of T7 and T23 transgenic mice was evaluated using 7,12-dimethylbenz(a)anthracene (DMBA), a carcinogen that causes lung and skin tumours[13]. Only 33% of T23 mice developed tumours in contrast to 100% of wild-type animals (Fig. 2a). Reductions in both skin and lung tumour incidence contributed to this decline (Fig. 2a). Tumour formation in T7 animals was not significantly reduced. Next, we examined the impact of moderate and high BubR1 overexpression on lung tumour formation in $Kras^{LA1}$ mice[14]. $Kras^{LA1}$ mice carry a conditional oncogenic $Kras$ allele ($Kras^{G12D}$) that becomes active on intra-chromosomal homologous recombination. At 6 weeks, $Kras^{LA1}$ mice had on average 17 lung tumours, whereas T23; $Kras^{LA1}$

mice had only 8 (Fig. 2b). Again, the moderately expressed T7 transgene failed to reduce tumour formation (Supplementary Fig. S2a), indicating that tumour protection requires a threshold of BubR1 overexpression.

Aneuploidy is a hallmark of human cancers, and aneuploidy-prone mouse models indicate that this condition is causally implicated in tumour development[15–17]. This, combined with the observation that oncogenic Ras promotes chromosome missegregation[18], led us to propose that BubR1 overexpression suppresses tumorigenesis by counteracting Ras-mediated aneuploidization. To test this notion, we transduced wild-type and T23 MEFs with a retrovirus expressing oncogenic Ras (Fig. 2c) and performed chromosome counts on day 5 post-infection. Indeed, BubR1 overexpression markedly decreased Ras-induced aneuploidy (Fig. 2d), which correlated with reduced chromosome missegregation (Fig. 2e). Next, we examined whether increased BubR1 also inhibits aneuploidization in lung tissue of $Kras^{LA1}$ mice. Acquisition of oncogenic Ras in lung produced a hyperplastic epithelium (Supplementary Fig. S2b), which on fluorescence *in situ*
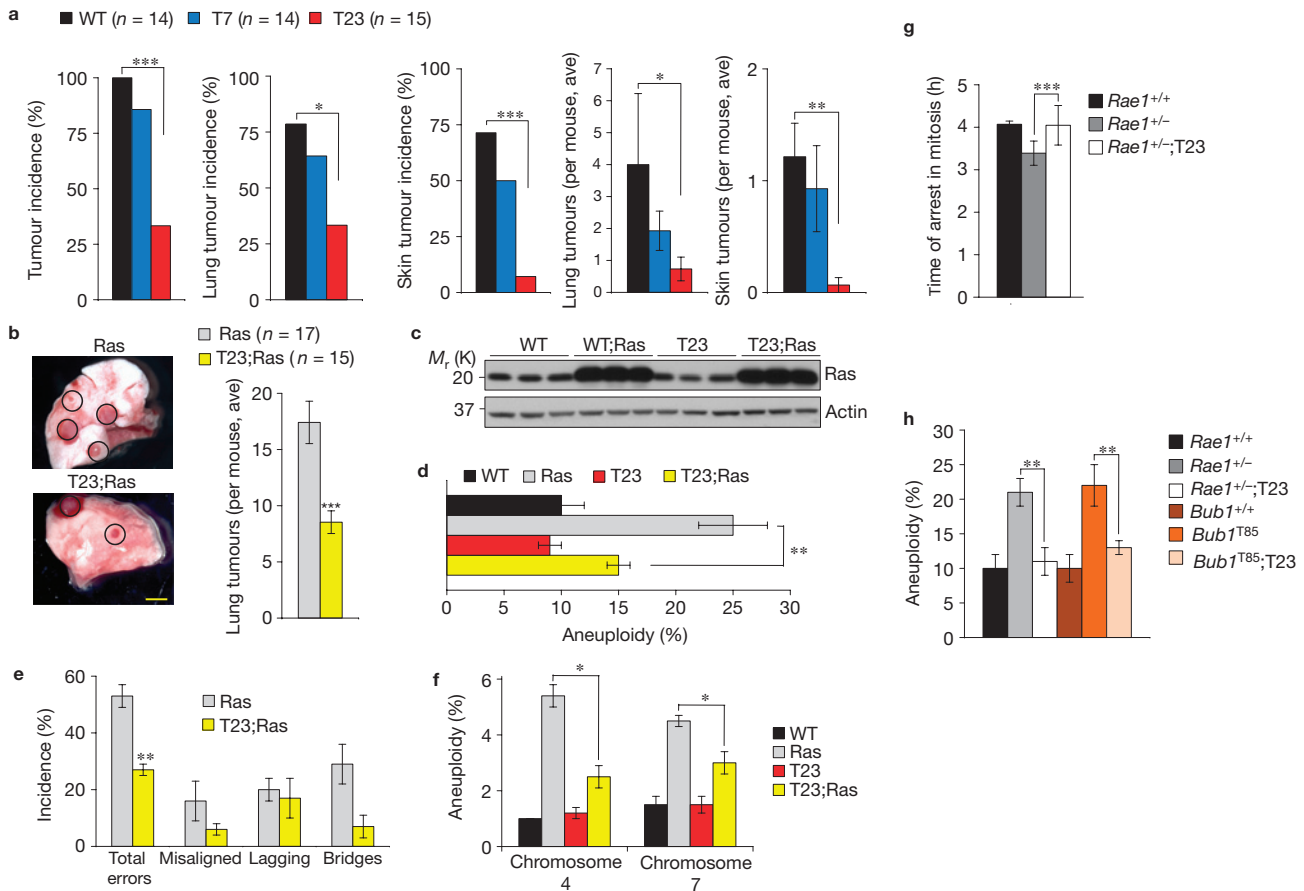
Figure 2 Resistance to tumorigenesis and chromosomal instability in BubR1 transgenic mice. (**a**) Tumour incidence and multiplicity in animals treated with DMBA on dorsal skin on postnatal day 5 and biopsied at 5 months of age. WT, wild type. Values represent means ± s.e.m. (**b**) Resistance of BubR1 transgenic mice to lung tumours (circled) induced by oncogenic Kras (G12D). Cohorts of $Kras^{LA1}$ and T23; $Kras^{LA1}$ mice were killed at 6 weeks of age and lung tumours counted under a dissection microscope. Values represent means ± s.d. Scale bar, 2 mm. (**c**) Western blots of cell extracts from wild-type and T23 MEFs with and without retrovirally expressed oncogenic Hras (G12V). Actin was used as a loading control. (**d,e**) Oncogenic Hras-induced aneuploidy (**d**) and chromosome missegregation (**e**) rates of MEF lines with and without BubR1 overexpression ($n = 3$ independent MEF lines each). Values represent means ± s.d. in **d** and means ± s.e.m. in **e**. (**f**) Aneuploidy rates in lungs of wild-type and $Kras^{LA1}$ mice with and without BubR1 overexpression. $n = 3$ mice for wild type and T23, and $n = 4$ for Ras and T23;Ras. Values represent means ± s.e.m. (**g**) Nocodazole-challenge assay showing that elevated BubR1 expression restores normal mitotic checkpoint activity in MEFs with low amounts of Rae1. Values represent means ± s.d. Three independent MEF lines per genotype were used. (**h**) Aneuploidy rates of mutant MEF lines with and without BubR1 overexpression ($n = 5$ MEF lines each). Values represent means ± s.d. *$P < 0.05$, **$P < 0.01$, ***$P < 0.001$. n indicates the number of mice (mixed gender) used per genotype in **a,b**. Uncropped images of blots are shown in Supplementary Fig. S6.

hybridization (FISH) analysis for chromosomes 4 and 7 showed increased aneuploidy (Fig. 2f). Aneuploidy was significantly reduced in T23; $Kras^{LA1}$ mice (Fig. 2f), but not in T7; $Kras^{LA1}$ mice (Supplementary Fig. S2c), indicating that protection against tumorigenesis by high levels of BubR1 tightly correlates with reduced aneuploidization.

To determine how high BubR1 levels counteract aneuploidization we focused on its known roles in mitotic checkpoint control and the establishment of proper microtubule–kinetochore attachments[2,3,12,19]. Mutant MEFs with low amounts of Rae1 have impaired mitotic checkpoint activity and are prone to chromosome segregation errors and aneuploidization[20]. On a T23 background, however, these MEFs had much lower missegregation and aneuploidy rates, which coincided with restoration of normal mitotic checkpoint activity (Fig. 2g,h and Supplementary Fig. S2d). $Bub1^{T85}$ MEFs, which overexpress the mitotic checkpoint protein Bub1, have an intact mitotic checkpoint but are predisposed to chromosome missegregation and aneuploidy due

to defective attachment error correction[12]. BubR1 overabundance markedly improved error correction in these MEFs, resulting in decreased aneuploidy (Fig. 2h and Supplementary Fig. S2d). Together, these findings indicate that increased BubR1 expression can preserve genomic integrity by ameliorating defects that perturb the mitotic checkpoint and/or kinetochore–microtubule attachment.

To analyse the impact of sustained high BubR1 expression on spontaneous tumorigenesis, we generated a cohort of T23 transgenic mice. As control cohorts, we used non-transgenic littermates and a transgenic strain expressing EGFP under the control of the CAGGS promoter, referred to as T-GFP mice. In accordance with conclusions from the DMBA and $Kras^{LA1}$ studies, development of lethal tumours (that is, malignant lymphomas, sarcomas and carcinomas) was significantly delayed in T23 mice, revealing a broad tumour protective effect of high BubR1 (Fig. 3a). The spontaneous tumours that developed in T23 animals contained low amounts of Flag–BubR1
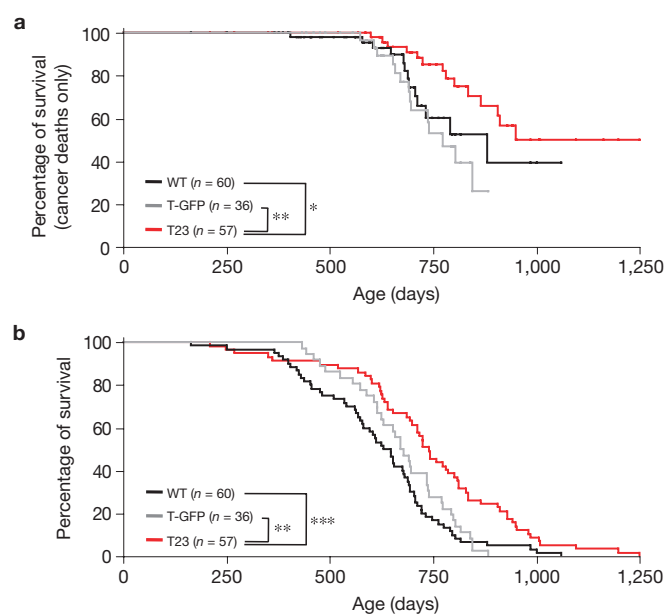
Figure 3 Increased BubR1 expression protects against spontaneous tumours and extends lifespan. (**a**) Survival curves of wild-type, T-GFP and T23 mice dying of cancer. Only mice with malignant lymphomas, sarcomas and carcinomas are included. Statistical analysis of the survival curves is represented by the asterisks (log-rank test). (**b**) Overall survival curves of wild-type, T-GFP and T23 mice. Note that the maximum lifespan of T23 mice was also significantly extended when compared with both wild-type and T-GFP control mice ($P = 0.05$ and 0.0056), respectively; one-sided Wang/Allison test referring to the proportion of mice alive at the 90th percentile survival point. Furthermore, note that the median lifespan of our wild-type cohort is similar to that of an earlier, independent study performed at the same site[40]. *$P < 0.05$, **$P < 0.01$, ***$P < 0.001$. n indicates the number of mice (mixed gender) per genotype.

(Supplementary Fig. S3a,b), implying that tumorigenesis selected for loss of transgene expression. Consistent with attenuated tumour development, T23 mice showed increased longevity (Fig. 3b). Tumour protection and lifespan extension were observed in both genders, although more profoundly in males (Supplementary Fig. S3c–f).

To explore whether high-level BubR1 expression has anti-ageing effects independent of tumour protection, we analysed T23 and wild-type mice for distinct parameters of healthspan. Muscle loss is a hallmark of ageing in both humans and rodents. In contrast to wild-type mice, which showed a 35% decrease in gastrocnemius muscle fibre diameter between 3 and 24 months of age, T23 mice were protected from muscle fibre atrophy (Fig. 4a). Relative gastrocnemius muscle weights of aged T23 mice were significantly larger than those of corresponding control mice (Supplementary Fig. S4a). Consistent with reduced muscle degeneration, ageing-induced upregulation of $p16^{Ink4a}$ and $p19^{Arf}$, two biomarkers of senescence and ageing[21], was blunted in the gastrocnemius of T23 mice (Fig. 4b,c). T23 mice outperformed wild-type counterparts in treadmill exercise tests (Fig. 4d–f), validating preservation of muscle function. Furthermore, renal sclerosis with glomerulosclerosis, interstitial fibrosis and tubular atrophy, which occurs with ageing, was reduced in 24-month-old T23 animals (Fig. 4g,h). Blood urea nitrogen levels of these animals were significantly lower than in age-matched wild-type animals (16.10 ± 1.95 mg dl^{-1} versus 23.02 ± 2.08 mg dl^{-1}, respectively, $P = 0.0136$,

unpaired t-test), indicating enhanced preservation of renal function. Ageing of kidney is characterized by accumulation of cells with γ-H2AX foci[22,23], which are thought to represent senescent cells. The foci themselves represent sites of DNA damage, potentially resulting from aberrant sister chromatid segregation during mitosis[24,25]. Consistent with reduced age-related pathology, kidneys of 24-month-old T23 animals contained significantly fewer cells with γ-H2AX foci than those of age-matched control mice (Fig. 4i). Conversely, the incidence of cells with γ-H2AX foci in kidneys of progeroid $BubR1$ mice was markedly increased at 3 months of age (Fig. 4i), indicating that formation of DNA double-strand breaks (DSBs) inversely correlates with the level of BubR1 expression. Reactive oxygen species (ROS) have been linked to age-related DNA damage[26], but we found no evidence for alterations in the abundance of or tolerance to ROS in T23 mice (Supplementary Fig. S4b–d). Decreased accumulation of cells with γ-H2AX foci in kidney of 24-month-old T23 mice correlated with increased BrdU incorporation, further supporting the idea that elevated BubR1 attenuates senescence-associated replicative arrest (Supplementary Fig. S4e).

BubR1 progeroid mice are thought to succumb to early death due to heart failure[27], prompting us to examine whether sustained BubR1 expression improves cardiac performance. In a cardiac stress tolerance test, in which mice are injected with a lethal dose of the β-adrenergic agonist isoproterenol, wild-type mice suffered cardiac arrest within 6.5 min (Fig. 4j). Consistent with reduced cardiac stress resistance, 5-month-old $BubR1^{H/H}$ mice died three times faster than control animals. In contrast, the time to death was significantly extended in T23 animals. Furthermore, whereas cardiac stress tolerance of wild-type mice significantly declined between 5 and 15 months of age, T23 mice retained high cardiac performance. Age-related interstitial fibrosis in heart tissue was markedly lower in T23 mice (Fig. 4k), corroborating that BubR1 overexpression acts to preserve cardiac function and structural integrity. Attenuated deterioration of skeletal muscle and heart in T23 mice was not characterized by increased stem cell abundance within these tissues (Fig. 4l). T23 animals also showed resistance to age-related retinal atrophy (Supplementary Fig. S4f), which correlated well with increased BubR1 expression in eye (Supplementary Fig. S1c). In contrast, osteoporosis and cataractogenesis, two other age-related disorders that we screened for, were not delayed (Supplementary Fig. S4g–i), indicating that the anti-ageing effect of increased BubR1 expression is confined to particular cell and tissue types.

Aneuploidy increases with ageing in mouse splenocytes[28]. To determine whether age-related aneuplodization also occurs in other tissues and correlates with age-related tissue dysfunction, we performed interphase FISH for chromosomes 4 and 7 on tissues of 3- and 24-month-old wild-type and T23 mice. Aneuploidy rates for both chromosomes markedly increased with ageing in wild-type lung tissue, but not in T23 lungs (Table 1). Similar data were obtained for tissues that exhibited characteristics of delayed ageing in T23 mice, including skeletal muscle, kidney, eye and heart (Table 1). The presence of age-related aneuploidy in wild-type heart was surprising, given that traditionally heart has been viewed as a terminally differentiated post-mitotic organ. However, recent studies indicate that the heart replaces its cells several times during its lifespan[29]. Inhibition of age-related aneuploidization was not universal as bone marrow and
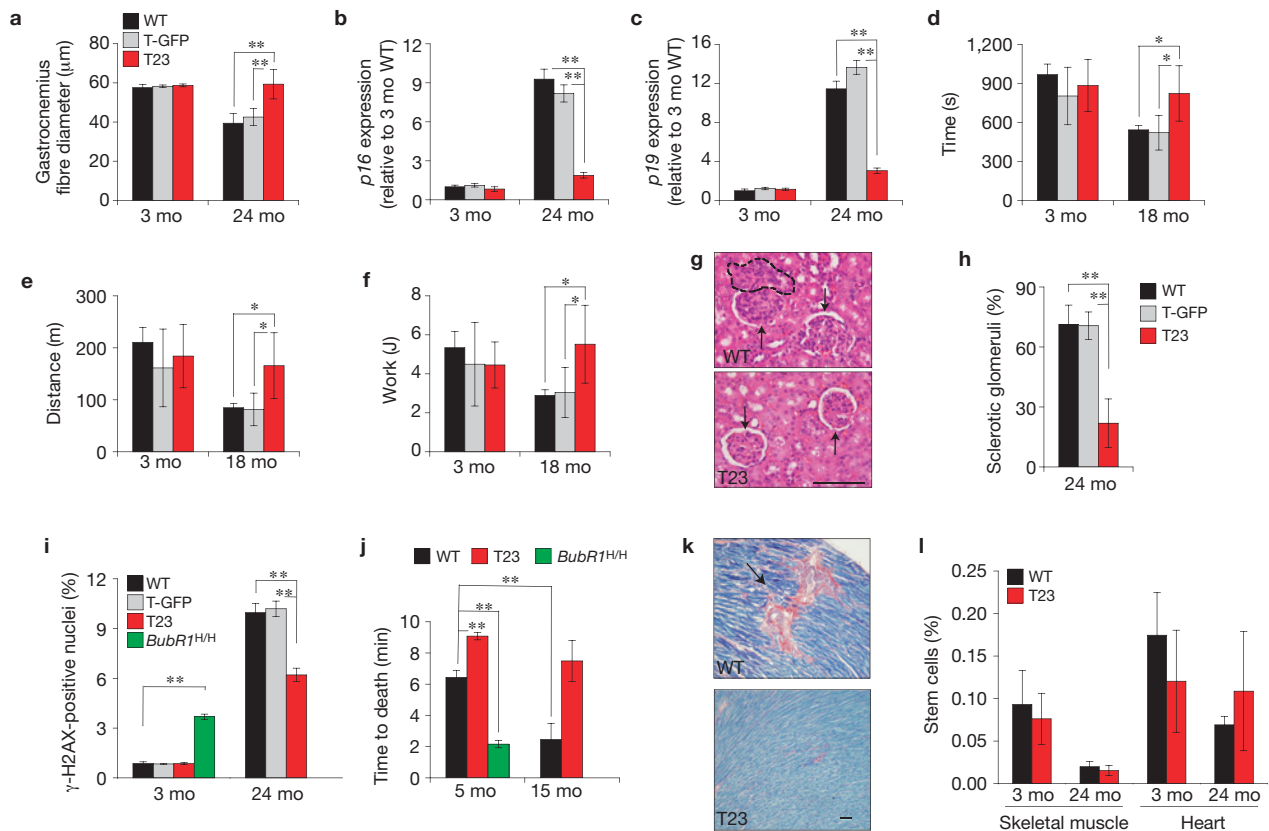
Figure 4 Increased BubR1 expression delays select age-related pathologies. (**a**) Sustained BubR1 expression attenuates muscle fibre atrophy. Gastrocnemius muscle fibre diameter declines with age in all genotypes except T23. WT, wild type. (**b**) Quantitative rtPCR analysis of $p16^{Ink4a}$ expression in gastrocnemius muscles of 3- and 24-month-old transgenic and control mice relative to 3-month-old wild-type muscles. (**c**) The same as in **b**, but for $p19^{Arf}$. (**d**–**f**) Exercise ability is enhanced in aged T23 mice. Time (**d**), distance (**e**) and work performed (**f**) are all improved in 18-month-old T23 animals when compared with wild-type and T-GFP animals. (**g**) Haematoxylin–eosin-stained kidney sections of 24-month-old mice. The area outlined by the dashed line depicts interstitial inflammation; arrows denote glomerular hypercellularity of wild-type mice (top) and normal glomeruli of T23 mice (bottom). Scale bar, 100 μm. (**h**) Percentage of sclerotic glomeruli from 24-month-old kidney sections. Forty glomeruli were scored for each animal. (**i**) DNA damage, as measured by γ-H2AX staining on cryosections of kidney tissue, is increased in $BubR1^{H/H}$ mice at a young age and reduced in transgenic mice at advanced age. (**j**) Cardiac stress tolerance correlates with BubR1 level of expression. (**k**) Ptah-stained heart sections of 24-month-old wild-type and T23 mice. Interstitial fibrosis (pink area) is significantly reduced in T23 animals. Scale bar, 50 μm. For all analyses in **a**–**k**, $n = 5$ males per genotype per age group. Error bars represent s.d. (**l**) Quantification of the percentage of stem cells isolated from 3- and 24-month-old wild-type and T23 mouse skeletal muscle (satellite cells) and heart (cardiac stem cells). $n = 3$ males per genotype per tissue. Values represent means ± s.e.m. Note that there are no significant differences between wild-type and T23. $*P < 0.05$, $**P < 0.01$, $***P < 0.001$.

small intestine, two tissues with a relatively high mitotic index, showed similar age-related aneuploidy rates in T23 and wild-type mice (Table 1). Notably, stem cells in skeletal muscle, heart and bone marrow showed resistance to age-related aneuploidization in both wild-type and T23 animals (Table 1), suggesting that these populations are well protected against whole-chromosome instability. There are several plausible mechanisms for why aneuploidy rates of differentiated cells could be high with stem cell aneuploidy being low (Supplementary Fig. S5k). First, lineage-primed progenitors derived from stem cells undergo multiple rounds of division before differentiation occurs and aneuploidization might occur during this proliferative phase. Second, it is possible that aneuploidy does occur when stem cells divide, but that the daughter cell that inherits stemness dies whereas the progenitor daughter cell survives and continues to proliferate. A third possibility would be that aneuploidization of differentiated cells is due to polyploidy resulting from fusion of nuclei. Polyploid nuclei, however, were not observed or extremely rare in our samples (data not shown).

Finally, age-related aneuploidization and tissue dysfunction were not attenuated in T7 mice (Supplementary Fig. S5), indicating that both beneficial effects require a certain threshold of BubR1 overexpression.

Our data here show that sustained high expression of BubR1 in mice protects against cancer, attenuates age-related deterioration of select tissues and extends median and maximum lifespan. We show that these beneficial effects tightly correlate with reduced oncogene-induced or age-related aneuploidization, and that high BubR1 levels act to reinforce mitotic checkpoint control and attachment error correction in the presence of genetic defects that cause mitotic stress. On the basis of these findings, it is tempting to speculate that high-level BubR1 expression extends health- and lifespan by attenuating chromosomal instability. Consistent with this hypothesis, many mouse models of accelerated aneuploidization are prone to tumorigenesis[15,30,31]. On the other hand, whereas BubR1 hypomorphic and Bub3/Rae1 double haploinsufficient mice exhibit overt premature ageing phenotypes[1,32], other aneuploidy-prone mouse strains do not. One possibility is

Table 1 Improved healthspan of T23 tissues correlates with reduced aneuploidization with age.

| Tissue or stem-cell type | Percentage of aneuploidy (s.d.) | | | |
| | 3-mo-old mice | | 24-mo-old mice | |
	Chr. 4	Chr. 7	Chr. 4	Chr. 7
WT lung	1.7 (0.6)	1.7 (0.6)	3.7 (0.6) }*	4.0 (0.0) }**
T23 lung	1.3 (0.6)	1.7 (0.6)	1.3 (0.6)	1.3 (0.6)
WT skeletal muscle	3.3 (0.6)	2.7 (0.6)	13.0 (1.2) }*	14.0 (1.7) }*
T23 skeletal muscle	3.3 (0.6)	2.7 (1.2)	7.3 (1.5)	8.0 (1.7)
WT kidney	1.7 (0.6)	1.3 (0.6)	5.7 (0.6) }*	7.3 (1.5) }*
T23 kidney	1.7 (0.6)	1.7 (0.6)	2.7 (1.5)	2.3 (2.0)
WT heart	2.3 (1.2)	2.7 (0.6)	11.3 (3.2) }*	11.3 (1.2) }**
T23 heart	2.3 (1.5)	2.0 (1.0)	5.3 (1.2)	6.0 (1.0)
WT eye	2.3 (0.6)	2.7 (0.6)	9.3 (1.5) }**	8.0 (1.0) }**
T23 eye	1.7 (0.6)	2.3 (0.6)	4.7 (0.6)	4.7 (0.6)
WT Spleen	1.3 (0.6)	1.3 (0.6)	3.3 (1.2)	4.7 (0.6)
T23 spleen	1.7 (1.2)	1.7 (1.2)	2.7 (0.6)	3.0 (1.0)
WT bone marrow	1.7 (0.6)	2.0 (1.0)	5.0 (1.0)	3.0 (1.0)
T23 bone marrow	1.7 (1.2)	2.0 (1.0)	4.3 (0.6)	4.0 (1.0)
WT small intestine	1.7 (0.6)	1.7 (0.6)	4.3 (0.6)	4.7 (0.6)
T23 small intestine	2.0 (1.0)	1.7 (0.6)	5.0 (1.0)	5.3 (1.2)
WT satellite cells	2.9 (0.1)	3.3 (0.7)	3.7 (1.1)	4.8 (1.8)
T23 satellite cells	2.1 (0.2)	3.5 (1.3)	3.5 (1.4)	5.1 (2.2)
WT cardiac stem cells	2.7 (0.6)	2.3 (0.6)	4.0 (1.0)	3.3 (0.6)
T23 cardiac stem cells	2.3 (0.6)	2.7 (0.6)	3.3 (0.6)	3.7 (1.2)
WT haematopoietic stem cells	1.3 (0.6)	1.7 (0.6)	2.3 (0.6)	3.0 (1.0)
T23 haematopoietic stem cells	1.7 (0.6)	2.0 (1.0)	2.0 (1.0)	2.3 (0.6)

Interphase FISH analysis on 3- and 24-month-old wild-type (WT) and T23 mice. $n = 3$ males per genotype, per tissue, per age group. Values represent means $\pm$ s.d. $*P < 0.05$, $**P < 0.01$. Numbers indicated in red represent values at 24 months that were significantly higher than the same chromosome when analysed at 3 months of age ($P < 0.05$).

that aneuploidy is required, but not sufficient for induction of age-related pathologies. For instance, aneuploidy may contribute to the induction of age-related pathologies only in the presence of other age-associated damage, such as DNA DSBs, mitochondrial DNA damage and proteotoxic damage[33,34]. Our observation that DSBs, which can result from specific types of chromosome segregation error[26,27], were increased in kidney of BubR1 progeroid mice and decreased in kidney of T23 transgenics (Fig. 4i), supports this notion.

Alternatively, the beneficial effects of sustained overexpression of BubR1 could be independent of chromosome segregation. BubR1 is normally present throughout the cell cycle and known to be implicated in roles outside mitosis, including DNA repair and ciliogenesis[35,36]. Furthermore, recent studies uncovered that APC/C^{Cdc20}, whose E3 ubiquitin ligase activity is controlled by BubR1, regulates important biological processes in post-mitotic cells such as morphogenesis and differentiation[37–39]. These findings raise the interesting possibility that BubR1 overexpression might exert its beneficial effects by controlling the stability of interphase APC/C^{Cdc20} substrates implicated in the suppression of cellular stresses that engage cellular senescence or other ageing-related pathways.

We provide experimental evidence that overexpression of a mitotic regulator can improve ploidy control, confer resistance to tumorigenesis and delay age-related decline in tissues and organs important to human health in the absence of apparent side effects. These findings identify BubR1 and its regulator(s) as unique and promising targets for treatment of a broad spectrum of aneuploid human cancers and key age-related disorders that dictate health. □

METHODS

Methods and any associated references are available in the online version of the paper.

Note: Supplementary Information is available in the online version of the paper

AUTHOR CONTRIBUTIONS

D.J.B., M.M.D., T.W., K.B.J., L.M., J.H.v.R., R.C.D., S.R., A.B., A.T., L.S., V.S. and J.M.v.D.designed and performed experiments, B.v.d.S. helped supervise T.W., and D.J.B. and J.M.v.D. wrote the manuscript. All authors discussed results, prepared figures and edited the manuscript.

1. Baker, D. J. et al. BubR1 insufficiency causes early onset of aging-associated phenotypes and infertility in mice. Nat. Genet. **36,** 744–749 (2004).
2. Lampson, M. A. & Kapoor, T. M. The human mitotic checkpoint protein BubR1 regulates chromosome-spindle attachments. Nat. Cell Biol. **7,** 93–98 (2005).
3. Malureanu, L. A. et al. BubR1 N terminus acts as a soluble inhibitor of cyclin B degradation by APC/C(Cdc20) in interphase. Dev. Cell **16,** 118–131 (2009).
4. Matsumoto, T. et al. Aging-associated vascular phenotype in mutant mice with low levels of BubR1. Stroke **38,** 1050–1056 (2007).
5. Hartman, T. K., Wengenack, T. M., Poduslo, J. F. & van Deursen, J. M. Mutant mice with small amounts of BubR1 display accelerated age-related gliosis. Neurobiol. Aging **28,** 921–927 (2007).
6. Baker, D. J. et al. Opposing roles for p16Ink4a and p19Arf in senescence and ageing caused by BubR1 insufficiency. Nat. Cell Biol. **10,** 825–836 (2008).
7. Matsuura, S. et al. Monoallelic BUB1B mutations and defective mitotic-spindle checkpoint in seven families with premature chromatid separation (PCS) syndrome. Am. J. Med. Genet. A **140,** 358–367 (2006).
8. Hanks, S. et al. Constitutional aneuploidy and cancer predisposition caused by biallelic mutations in BUB1B. Nat. Genet. **36,** 1159–1161 (2004).
9. Burtner, C. R. & Kennedy, B. K. Progeria syndromes and ageing: what is the connection? Nat. Rev. Mol. Cell Biol. **11,** 567–578 (2010).
10. Sotillo, R. et al. Mad2 overexpression promotes aneuploidy and tumorigenesis in mice. Cancer Cell **11,** 9–23 (2007).
11. Van Ree, J. H., Jeganathan, K. B., Malureanu, L. & van Deursen, J. M. Overexpression of the E2 ubiquitin-conjugating enzyme UbcH10 causes chromosome missegregation and tumor formation. J. Cell Biol. **188,** 83–100 (2010).
12. Ricke, R. M., Jeganathan, K. B. & van Deursen, J. M. Bub1 overexpression induces aneuploidy and tumor formation through Aurora B kinase hyperactivation. J. Cell Biol. **193,** 1049–1064 (2011).
13. Serrano, M. et al. Role of the INK4a locus in tumor suppression and cell mortality. Cell **85,** 27–37 (1996).
14. Johnson, L. et al. Somatic activation of the K-ras oncogene causes early onset lung cancer in mice. Nature **410,** 1111–1116 (2001).
15. Schvartzman, J. M., Sotillo, R. & Benezra, R. Mitotic chromosomal instability and cancer: mouse modelling of the human disease. Nat. Rev. Cancer **10,** 102–115 (2010).
16. Holland, A. J. & Cleveland, D. W. Boveri revisited: chromosomal instability, aneuploidy and tumorigenesis. Nat. Rev. Mol. Cell Biol. **10,** 478–487 (2009).
17. Baker, D. J., Jin, F., Jeganathan, K. B. & van Deursen, J. M. Whole chromosome instability caused by Bub1 insufficiency drives tumorigenesis through tumor suppressor gene loss of heterozygosity. Cancer Cell **16,** 475–486 (2009).
18. Saavedra, H. I. et al. The RAS oncogene induces genomic instability in thyroid PCCL3 cells via the MAPK pathway. Oncogene **19,** 3948–3954 (2000).
19. Sudakin, V., Chan, G. K. & Yen, T. J. Checkpoint inhibition of the APC/C in HeLa cells is mediated by a complex of BUBR1, BUB3, CDC20, and MAD2. J. Cell Biol. **154,** 925–936 (2001).
20. Babu, J. R. et al. Rae1 is an essential mitotic checkpoint regulator that cooperates with Bub3 to prevent chromosome missegregation. J. Cell Biol. **160,** 341–353 (2003).

21. Krishnamurthy, J. *et al*. Ink4a/Arf expression is a biomarker of aging. *J. Clin. Invest.* **114,** 1299–1307 (2004).

22. Herbig, U., Jobling, W. A., Chen, B. P., Chen, D. J. & Sedivy, J. M. Telomere shortening triggers senescence of human cells through a pathway involving ATM, p53, and p21(CIP1), but not p16(INK4a). *Mol. Cell* **14,** 501–513 (2004).

23. Matheu, A. *et al*. Delayed ageing through damage protection by the Arf/p53 pathway. *Nature* **448,** 375–379 (2007).

24. Lukas, C. *et al*. 53BP1 nuclear bodies form around DNA lesions generated by mitotic transmission of chromosomes under replication stress. *Nat. Cell Biol.* **13,** 243–253 (2011).

25. Janssen, A., van der Burg, M., Szuhai, K., Kops, G. J. & Medema, R. H. Chromosome segregation errors as a cause of DNA damage and structural chromosome aberrations. *Science* **333,** 1895–1898 (2011).

26. Vijg, J. & Campisi, J. Puzzles, promises and a cure for ageing. *Nature* **454,** 1065–1071 (2008).

27. Baker, D. J. *et al*. Clearance of p16Ink4a-positive senescent cells delays ageing-associated disorders. *Nature* **479,** 232–236 (2011).

28. Lushnikova, T., Bouska, A., Odvody, J., Dupont, W. D. & Eischen, C. M. Aging mice have increased chromosome instability that is exacerbated by elevated Mdm2 expression. *Oncogene* **30,** 4622–4631 (2011).

29. Bergmann, O. *et al*. Evidence for cardiomyocyte renewal in humans. *Science* **324,** 98–102 (2009).

30. Holland, A. J. & Cleveland, D. W. Losing balance: the origin and impact of aneuploidy in cancer. *EMBO Rep.* **13,** 501–514 (2012).

31. Pfau, S. J. & Amon, A. Chromosomal instability and aneuploidy in cancer: from yeast to man. *EMBO Rep.* **13,** 515–527 (2012).

32. Baker, D. J. *et al*. Early aging-associated phenotypes in Bub3/Rae1 haploinsufficient mice. *J. Cell Biol.* **172,** 529–540 (2006).

33. Li, H., Mitchell, J. R. & Hasty, P. DNA double-strand breaks: a potential causative factor for mammalian aging? *Mech. Ageing Dev.* **129,** 416–424(2008).

34. Morimoto, R. I. Proteotoxic stress and inducible chaperone networks in neurodegenerative disease and aging. *Genes Dev.* **22,** 1427–1438 (2008).

35. Fang, Y. *et al*. BubR1 is involved in regulation of DNA damage responses. *Oncogene* **25,** 3598–3605 (2006).

36. Miyamoto, T. *et al*. Insufficiency of BUBR1, a mitotic spindle checkpoint regulator, causes impaired ciliogenesis in vertebrates. *Hum. Mol. Genet.* **20,** 2058–2070 (2011).

37. Malureanu, L. *et al*. Cdc20 hypomorphic mice fail to counteract de novo synthesis of cyclin B1 in mitosis. *J. Cell Biol.* **191,** 313–329 (2010).

38. Kim, A. H. *et al*. A centrosomal Cdc20-APC pathway controls dendrite morphogenesis in postmitotic neurons. *Cell* **136,** 322–336 (2009).

39. Yang, Y. *et al*. A Cdc20-APC ubiquitin signaling pathway regulates presynaptic differentiation. *Science* **326,** 575–578 (2009).

40. Conover, C. A. & Bale, L. K. Loss of pregnancy-associated plasma protein A extends lifespan in mice. *Aging Cell* **6,** 727–729 (2007).

METHODS

Generation of Flag–mBubR1 transgenic mice. T7 and T23 BubR1 transgenic mice overexpressing Flag-tagged murine BubR1 protein were generated according to previously described methods[11,41]. T-GFP mice, which overexpress EGFP using the same promoter sequence as was used for the BubR1 transgene, were obtained and used as a control (stock number 004178, strain C57BL/6J, Jackson Laboratories). Note that EGFP levels in T-GFP and T23 mice were similar. Protocols used for PCR genotyping of the above strains are available on request. All mice were on a mixed C57BL/6-SV129 background and were housed in a pathogen-free barrier environment for the duration of the study. These animals were fed a 10%-fat diet and maintained on a 12 h light/dark cycle and were inspected daily. Animals in survival curves were mice found dead or euthanized if unlikely to survive for more than 48 h. These mice were carefully screened for tumours. Tumours were collected and processed by standard procedures for histopathological evaluation. Malignant lymphomas, sarcomas and carcinomas were considered in our tumour-free survival analysis. Note that animals used for experiments, including healthspan analyses, were omitted from the survival analysis. For light and fluorescence microscopy imaging of pups and organs we used a fluorescence dissecting microscope mounted with a camera (Leica). All images were taken within an hour of collection from an intra-cardially PBS-flushed mouse. Isoproterenol-challenge assays were performed on male mice. A lethal dose ($680 \, \text{mg kg}^{-1}$) was given to all animals and time until death was measured. All animal procedures were reviewed and approved by the Institutional Animal Care and Use Committee.

Statistical analyses. Prism software was used for the generation of all survival curves and statistical analysis. Log-rank tests were used to determine overall and pairwise significance for all survival curves (Fig. 3 and Supplementary Fig. S3c–f). Log-rank tests were also used in Fig. 2g and Supplementary Fig. S4b,i. One-sided Wang–Allison tests were used to determine maximum lifespan changes[42] in Fig. 3 and Supplementary Fig. S3c–f. Chi-squared tests for overall and pairwise significance were used for overall, lung and skin tumour incidence (Fig. 2a, first three graphs). Mann–Whitney tests were used for pairwise significance analysis in the following figures: Fig. 2a (graphs for average number of tumours); Figs 2b,f,h, 4a–c,h–j and Supplementary Figs S2a,c, S4e–h and S5a–c,g–i. Kruskal–Wallis tests for overall significance were performed before conducting these Mann–Whitney tests. An unpaired t-test was used for pairwise comparisons in the following figures: Figs 1d–f, 2d,e, 4d–f,l and Table 1 and Supplementary Figs S2d, S4a,c,d and S5d–f,j.

Western blot analysis, immunoprecipitation and immunohistochemistry. Immunoprecipitations and western blot analysis were performed as previously described[43]. Mitotic cell lysates were prepared as described previously[3]. Tissue lysates were prepared by first snap-freezing the tissue sample in liquid nitrogen and then grinding it to powder form in mortar and pestle. Ten milligrams of the powder was suspended in 100 μl of 1× PBS and 100 μl of Laemmli lysis buffer and boiled for 10 min before loading into Tris–HCl polyacrylamide gel. Blots were probed with antibodies for P-H3$^{\text{Ser10}}$ (Millipore; 06-570, 1:500), BubR1 (ref. 1; 1:1,000) Flag (Origene; TA100011, 1:1,000), β-actin (Sigma; A5441, 1:40,000), EGFP (Cell Signaling; 2,956, 1:1,000), Aurora B (BD Biosciences; 611083, 1:1,000), Cdc20 (1:1,000), Plk1 (1:500) and Hras (1:5,000; Santa Cruz Biotechnology; SC-8358, SC-17783 and SC-520, respectively), Bub3 (ref. 20; 1:1,000), Mad2 (ref. 11; 1:1,000) and Bub1 (ref. 44; 1:1,000). All antibodies were detected with secondary HRP-conjugated goat anti-mouse or anti-rabbit antibodies (Jackson Immunoresearch; 1:10,000). Equal loading was confirmed by using α-tubulin (Sigma; T9026, 1:2,000) or by Ponceau S staining. Immunohistochemistry for BubR1 (BD Biosciences; 612503, 1:500) was performed on formalin-fixed, paraffin-embedded lung tumour sections using the SignalStain Boost IHC detection reagent as per the manufacturer's instructions (Cell Signaling).

Generation and culture of MEFs and live-cell imaging. Wild-type, T7 and T23 MEFs were generated and cultured as previously described[1]. Double-mutant MEFs were produced by breeding T23 transgenic females to $Rae1^{+/-}$ (ref. 20) and $Bub1^{T85}$ males[12]. Live-cell imaging-based analyses of chromosome segregation errors and mitotic checkpoint activity were as previously described[11]. Nocodazole- and taxol-challenge assays and mitotic timing experiments were performed as previously described[3]. Oncogenic Ras was expressed in passage 3 (P3) wild-type and T23 MEFs using pBabe puro $Hras^{\text{G12V}}$ (Addgene plasmid 9051). Puromycin-resistant MEFs ($2 \, \mu\text{g ml}^{-1}$ puromycin) were analysed by live-cell imaging five days post-transduction. At least three independent MEF lines per genotype were used in all experiments.

Karyotype analyses. Splenocyte and MEF karyotype analyses were performed as described previously[20]. FISH analysis on single cells isolated from fresh lung tissue was performed as described previously[6]. Chromosome counts on MEFs expressing oncogenic Ras were done as follows: P3 wild-type and T23 MEFs were transduced with pBabe puro $Hras^{\text{G12V}}$ for two days, cultured in medium containing $2 \, \mu\text{g ml}^{-1}$ puromycin for two days and arrested in mitosis with colcemid on day 5. Interphase FISH analysis on cell suspensions prepared from various wild-type, T7 and T23 tissues was performed as previously described[17] in the Mayo Clinic Cytogenetics Core Facility as described in detail in ref. 45. At least 100 cells were analysed per sample, $n \geq 3$ samples per genotype and tissue.

Tumour susceptibility studies. DMBA treatment of mice was performed as previously described[13]. $K\text{-ras}^{\text{LA1}}$ mice[14] were obtained from the MMHCC (NCI Frederick).

Age-related phenotyping. Biweekly, mice were screened for overt cataracts[32]. Muscle fibre diameter measurements were taken on gastrocnemius muscles as previously described[6]. Exercise ability assessments were performed as described previously[27]. Individual gastrocnemius muscles were isolated from 18-month-old female mice. The relative weight is the weight of one gastrocnemius muscle divided by the overall body mass. Bone mineral density and bone mineral content were determined using DEXA (dual-energy X-ray absortiometry) scanning. Formalin-fixed, paraffin-embedded kidney samples were stained using routine haematoxylin and eosin staining. Forty randomly selected glomeruli were scored for sclerosis. Glomeruli with >50% sclerosis were determined to be sclerotic. Blood urea nitrogen assays were performed on 24-month-old mice as described previously[46]. Ptah staining on formalin-fixed, paraffin-embedded heart samples was performed as described previously[47]. Retinal thickness was determined by measuring the thickness of the retinal layer in haematoxylin–eosin-stained paraffin-embedded eye tissue using a calibrated computer program (Olympus MicroSuite 5). Forty random measurements were taken for each sample. γ-H2AX staining was performed as described previously[23].

Stem cell isolation and quantification. Satellite cells were labelled and purified as previously described[48]. Briefly, excised gastrocnemius muscles were washed in PBS and digested in DMEM containing collagenase type II solution (Worthington Biochemical) and 2% FCS for 45–60 min with agitation at 37 °C. Cell suspensions were filtered through a 45 μμ mesh and cells were centrifuged for 5 min at 500 g. Cells were incubated in blocking buffer for 15 min on ice following antibody staining for CD45, CD34 and Sca1 (all from BD-Biosciences; 557659, 560230 and 553336, respectively). Cells with a CD45$^-$, Sca-1$^-$ and CD34$^+$ surface profile[49] were collected using a FACS Aria Cell Sorter (BD Biosciences) running FACSDiva software. Enzymatic isolation of endogenous cardiac stem cells was performed after Langendorf perfusion of the heart[50] to obtain a viable single-cell suspension. Following antibody staining for c-Kit, CD45 and CD34, cells with a c-Kit$^+$, CD45$^-$ and CD34$^-$ surface profile were collected[51] (c-Kit antibody was from BD-Biosciences; 561075). Identification and quantification of haematopoietic stem cells was performed as described previously[52].

Quantitative rtPCR. Quantitative real-time PCR (rtPCR) analysis was performed on complementary DNA generated from RNA extracted from gastrocnemius muscle of 3-month-old and 24-month-old mice as previously described[6].

***In vivo* BrdU incorporation.** Analyses for *in vivo* BrdU incorporation were performed on 24-month-old mice as previously described[6].

Assessment of ROS resistance by paraquat. Paraquat (methyl viologen; Sigma) was dissolved in sterile saline and administered to 3- to 4-month-old mice by intraperitoneal injection at a dose of $60 \, \text{mg kg}^{-1}$ body weight. Animals were monitored for survival for 10 days following paraquat injection.

Hydrogen peroxide and DCFDA assay. Hydrogen peroxide (H_2O_2) levels in gastrocnemius muscle of 24-month-old mice were determined by using the Amplex Red Hydrogen Peroxide Assay Kit according to the protocol of the manufacturer (Invitrogen). Fluorescence signal was measured using an excitation wavelength of 545 nm and an emission wavelength of 590 nm. The H_2O_2 concentration per milligram of protein was calculated by using a standard curve. H_2O_2 levels were presented as relative to 24-month-old wild-type mice. ROS levels in liver of 24-month-old mice were analysed by using carboxy-DCFDA (2′,7′-dichlorodihydrofluorescein diacetate, Invitrogen). Tissue extracts were added

to DCFDA (25 µM) and fluorescence signal was measured using an excitation wavelength of 485 nm and an emission wavelength of 530 nm. For both experiments, the homogenization buffer consisted of 20 mM glycerolphosphate, 20 mM NaF, 2 mM sodium orthovanadate, 1 mM EDTA, 0.5 mM phenylmethyl sulphonyl fluoride, 1 µM pepstatin, 100 mM Tris–HCl (pH 7.4) and a freshly added mini EDTA-free cocktail tablet (Roche).

41. Van Ree, J., Zhou, W., Li, M. & van Deursen, J. M. Transgenesis in mouse embryonic stem cells. *Methods Mol. Biol.* **693,** 143–162 (2011).
42. Wang, C., Li, Q., Redden, D. T., Weindruch, R. & Allison, D. B. Statistical methods for testing effects on 'maximum lifespan'. *Mech. Ageing Dev.* **125,** 629–632 (2004).
43. Kasper, L. H. *et al.* CREB binding protein interacts with nucleoporin-specific FG repeats that activate transcription and mediate NUP98-HOXA9 oncogenicity. *Mol. Cell Biol.* **19,** 764–776 (1999).
44. Jeganathan, K., Malureanu, L., Baker, D. J., Abraham, S. C. & van Deursen, J. M. Bub1 mediates cell death in response to chromosome missegregation and acts to suppress spontaneous tumorigenesis. *J. Cell Biol.* **179,** 255–267 (2007).
45. Bayani, J. & Squire, J. A. Fluorescence *in situ* hybridization (FISH). *Curr. Protoc. Cell Biol.* 1–51 (2004).
46. Nath, K. A., Croatt, A. J., Warner, G. M. & Grande, J. P. Genetic deficiency of Smad3 protects against murine ischemic acute kidney injury. *Am. J. Physiol. Renal. Physiol.* **301,** F436–F442 (2011).
47. Ameri, A., Kurachi, S., Sueishi, K., Kuwahara, M. & Kurachi, K. Myocardial fibrosis in mice with overexpression of human blood coagulation factor IX. *Blood* **101,** 1871–1873 (2003).
48. Conboy, I. M., Conboy, M. J., Smythe, G. M. & Rando, T. A. Notch-mediated restoration of regenerative potential to aged muscle. *Science* **302,** 1575–1577 (2003).
49. Sherwood, R. I. *et al.* Isolation of adult mouse myogenic progenitors: functional heterogeneity of cells within and engrafting skeletal muscle. *Cell* **119,** 543–554 (2004).
50. Liu, X. K. *et al.* Genetic disruption of Kir6.2, the pore-forming subunit of ATP-sensitive K+ channel, predisposes to catecholamine-induced ventricular dysrhythmia. *Diabetes* **53** (Suppl. 3), S165–S168 (2004).
51. Oh, H. *et al.* Cardiac progenitor cells from adult myocardium: homing, differentiation, and fusion after infarction. *Proc. Natl Acad. Sci. USA* **100,** 12313–12318 (2003).
52. Pajerowski, A. G. *et al.* Adult hematopoietic stem cells require NKAP for maintenance and survival. *Blood* **116,** 2684–2693 (2010).
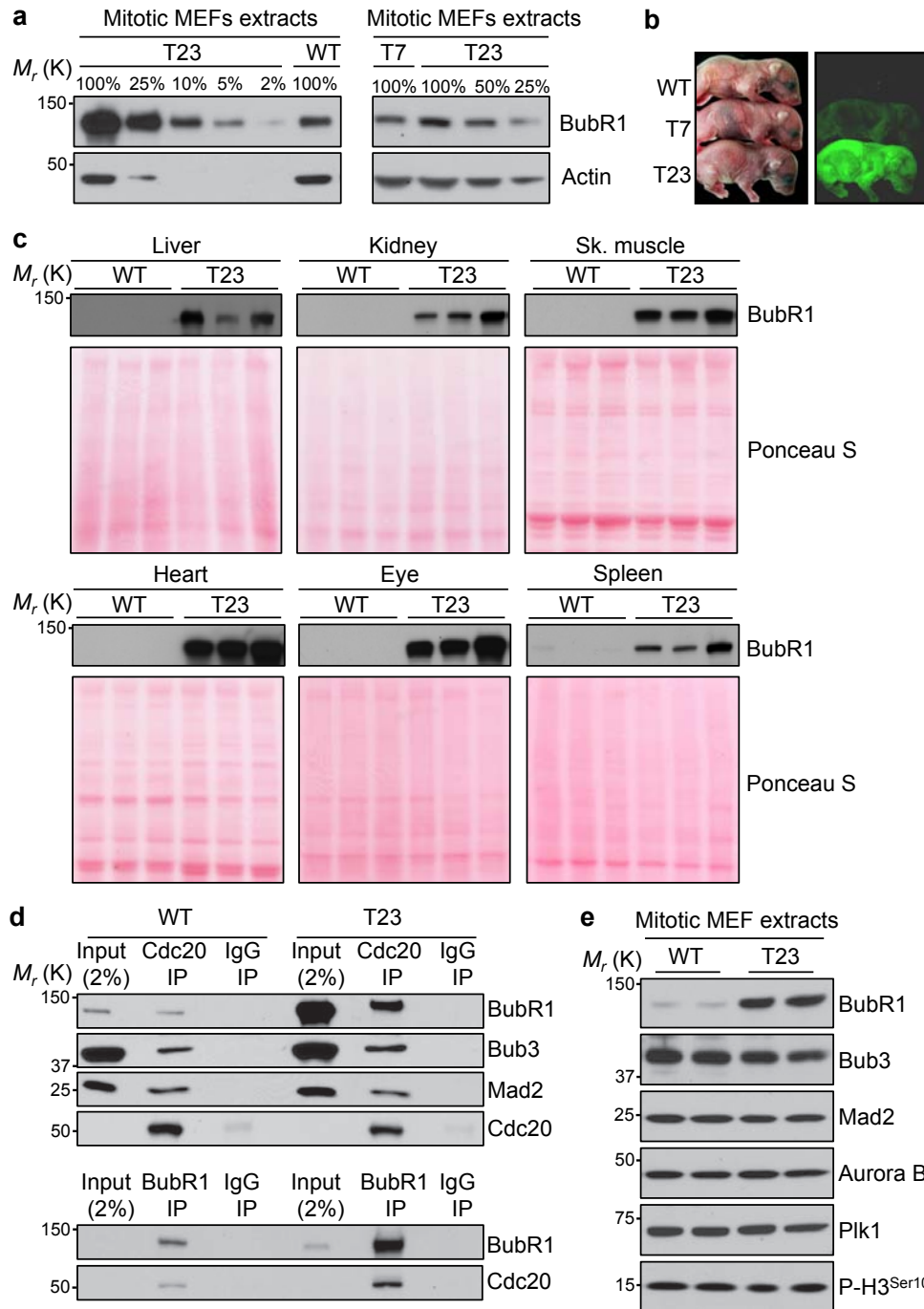
Figure S1 BubR1 expression analysis in T23 mouse tissues and analysis of mitotic checkpoint complex formation and levels of key mitotic regulators in T23 MEFs. (a) Western blot analysis of mitotic MEF extracts for BubR1. BubR1 protein levels in T23 MEFs were about 2-fold higher than in T7 MEFs and 10-fold higher than in wildtype MEFs. Actin served as a loading control. (b) Images of WT and transgenic pups obtained by light (left) and fluorescence microscopy (right). (c) The BubR1 transgene continues to be expressed late in life of transgenic animals and is not subject to silencing. Western blot analysis of tissues of 24-month-old WT and T23 mice. Blots were probed for BubR1. Ponceau S staining was used as a loading control. (d) Immunoblots of wildtype and T23 MEF extracts subjected to immunoprecipitation with the indicated antibodies. (e) Western blots of mitotic cell extracts of wildtype and T23 MEFs probed for key mitotic regulators. P-H3^{Ser10} was used as a control for equal loading of mitotic cells.
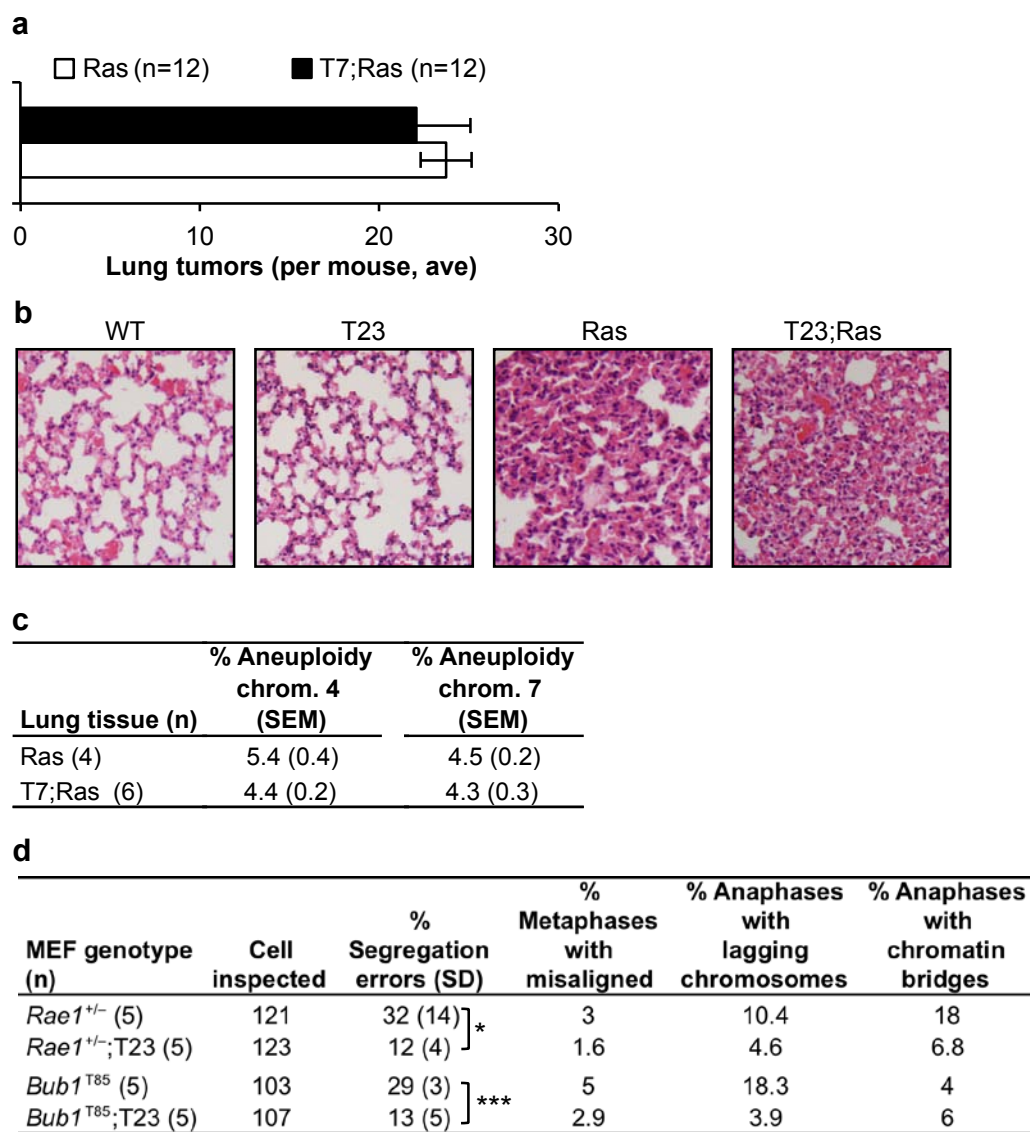
Supplementary Fig. S2 Baker et al.

a

□ Ras (n=12) ■ T7;Ras (n=12)

Lung tumors (per mouse, ave)

b

| WT | T23 | Ras | T23;Ras |

c

Lung tissue (n)	% Aneuploidy chrom. 4 aneuploidy (SEM)	% Aneuploidy chrom. 7 aneuploidy (SEM)
Ras (4)	5.4 (0.4)	4.5 (0.2)
T7;Ras (6)	4.4 (0.2)	4.3 (0.3)

d

MEF genotype (n)	Cell inspected	% Segregation errors (SD)	% Metaphases with misaligned	% Anaphases with lagging chromosomes	% Anaphases with chromatin bridges
Rae1^{+/−} (5)	121	32 (14) ⎤ *	3	10.4	18
Rae1^{+/−};T23 (5)	123	12 (4) ⎦	1.6	4.6	6.8
Bub1[T85] (5)	103	29 (3) ⎤ ***	5	18.3	4
Bub1[T85];T23 (5)	107	13 (5) ⎦	2.9	3.9	6

Figure S2 Protection against tumor formation and aneuploidization requires a threshold of BubR1 overexpression. **(a)** BubR1 T7 transgenic mice are not protected from lung tumors induced by oncogenic Kras (G12D). Cohorts of *Kras*[LA1], and T7;*Kras*[LA1] mice were killed at 6 weeks of age and lung tumors counted under a dissection microscope. Error bars indicate SEM. **(b)** Alveolar hyperplasia in *K-ras*[LA1] and T23;*K-ras*[LA1]; mice is similar. Haematoxylin-eosin stained lung sections of mice of the indicated genotypes (at 6 weeks of age). Hyperplastic alveolar tissue (without tumors) of *K-ras*[LA1] and T23;*K-ras*[LA1] mice is shown. Note that lung tissue of T23 transgenic mice is histologically normal. **(c)** Aneuploidy rates in lungs of *Kras*[LA1] mice with and without BubR1 clone T7 overexpression. **(d)** Chromosome missegregation rates of mutant MEF lines with and without BubR1 overexpression. Consistent with reduced aneuploidy rates, the fidelity of segregation is improved when BubR1 levels are high. $*P < 0.05$, $***P < 0.001$. n indicates the number of mice (mixed gender) used per genotype in **a** and **c**, and the number of independent MEF lines used in **d**.
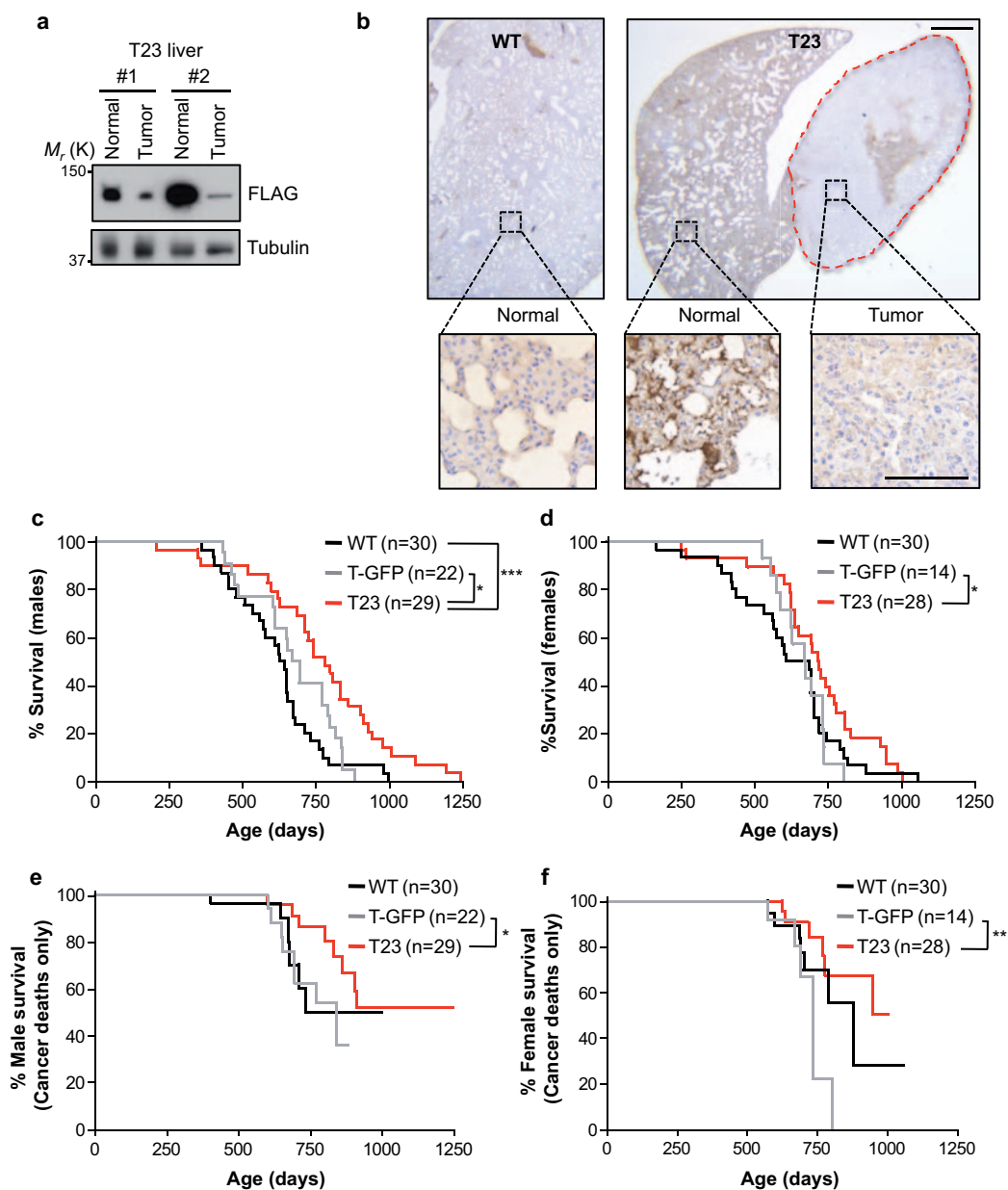
Figure S3 Overall and tumor-free survival of T23 animals is extended in both males and females. **(a, b)** Analysis of BubR1 protein levels in spontaneous tumors. **(a)** Western blot analysis of T23 liver tumors and flanking normal tissue for expression of transgenic BubR1 (FLAG-BubR1). Tubulin was used as a loading control. **(b)** Representative images of WT and T23 lung sections stained for BubR1. Note that BubR1 is present at high levels in normal lung tissue of T23 mice but not in neighboring tumor tissue. Scale bars: top, 1 mm; bottom, 100 μm. **(c-f)** Data presented are from the same mouse cohorts as in Fig. 4, but now separated by gender. **(c)** Overall survival of males and **(d)** females, and **(e)** tumor-free survival of males and **(f)** females. *$P < 0.05$, **$P < 0.01$, ***$P < 0.001$.
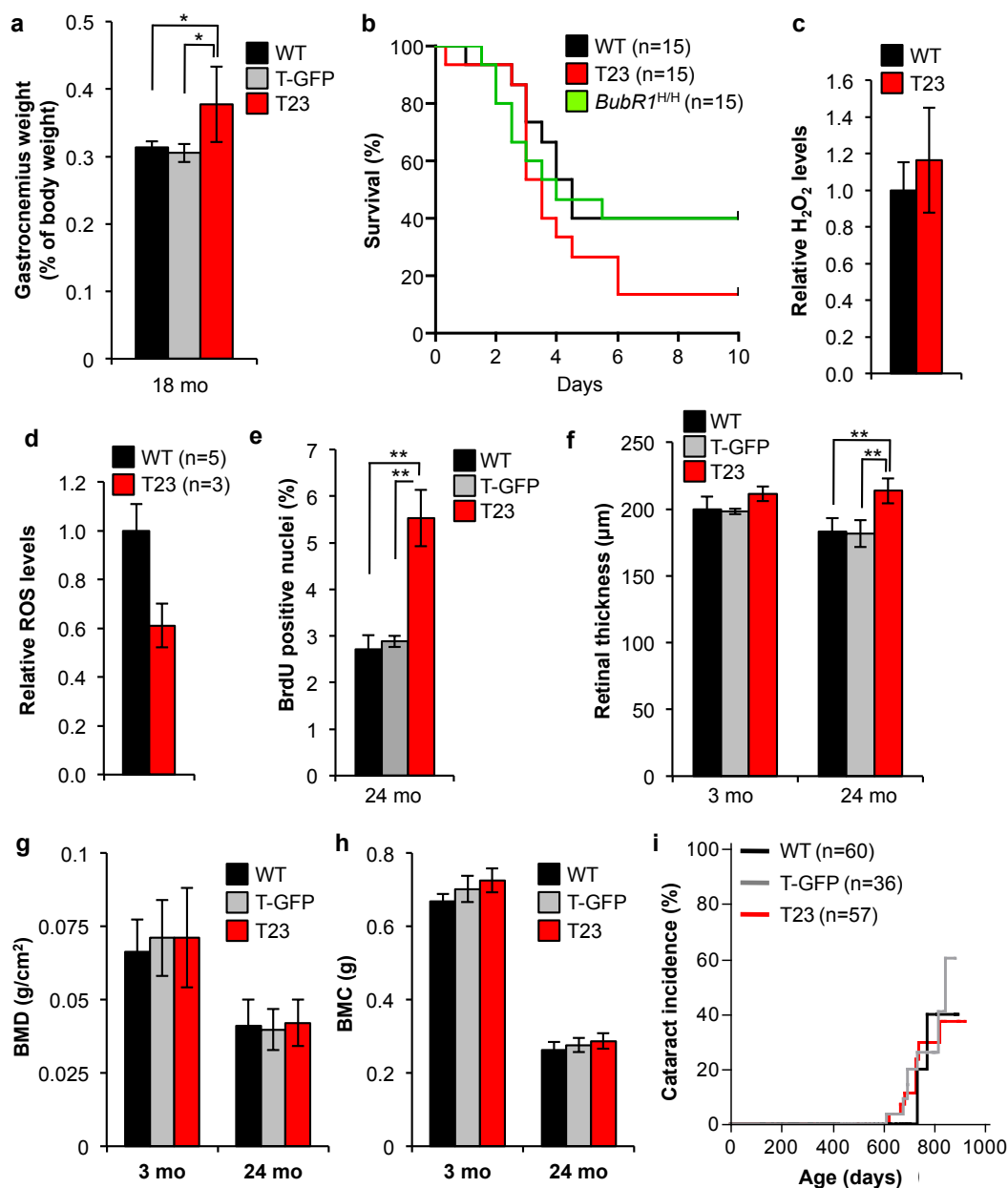
Figure S4 High levels of BubR1 delay age-related changes in a tissue specific manner. **(a)** BubR1 overexpression protects against loss of muscle mass. **(b)** Levels of BubR1 do not correlate with altered sensitivity to acute oxidative stress, as survival after paraquat injection in 3-4 month-old mice is unchanged. **(c)** H_2O_2 levels in gastrocnemius of 24-month-old mice in T23 is similar to wildtype. **(d)** Relative ROS levels are unchanged in livers of 24-month-old mice. **(e)** Proliferative capacity in kidney, as measured by BrdU incorporation, is increased in aged BubR1 transgenic mice. **(f)** Age-related retinal degeneration is prevented by high levels of BubR1. **(g-h)** High levels of BubR1 are unable to prevent osteoporosis. Bone mineral density **(g)** and bone mineral content **(h)** declines in mice with age. **(i)** Cataract onset and incidence are not prevented by overexpression of BubR1 in the eye. n=5 females per genotype in **a**, and 5 males per genotype in **c-h**. n in **b** and **i** indicates the number of mice (mixed gender) used per genotype. Values in **a** and **e-h** are means ± SD, values in **c** and **d** are means ± SEM. *$P < 0.05$, **$P < 0.01$.
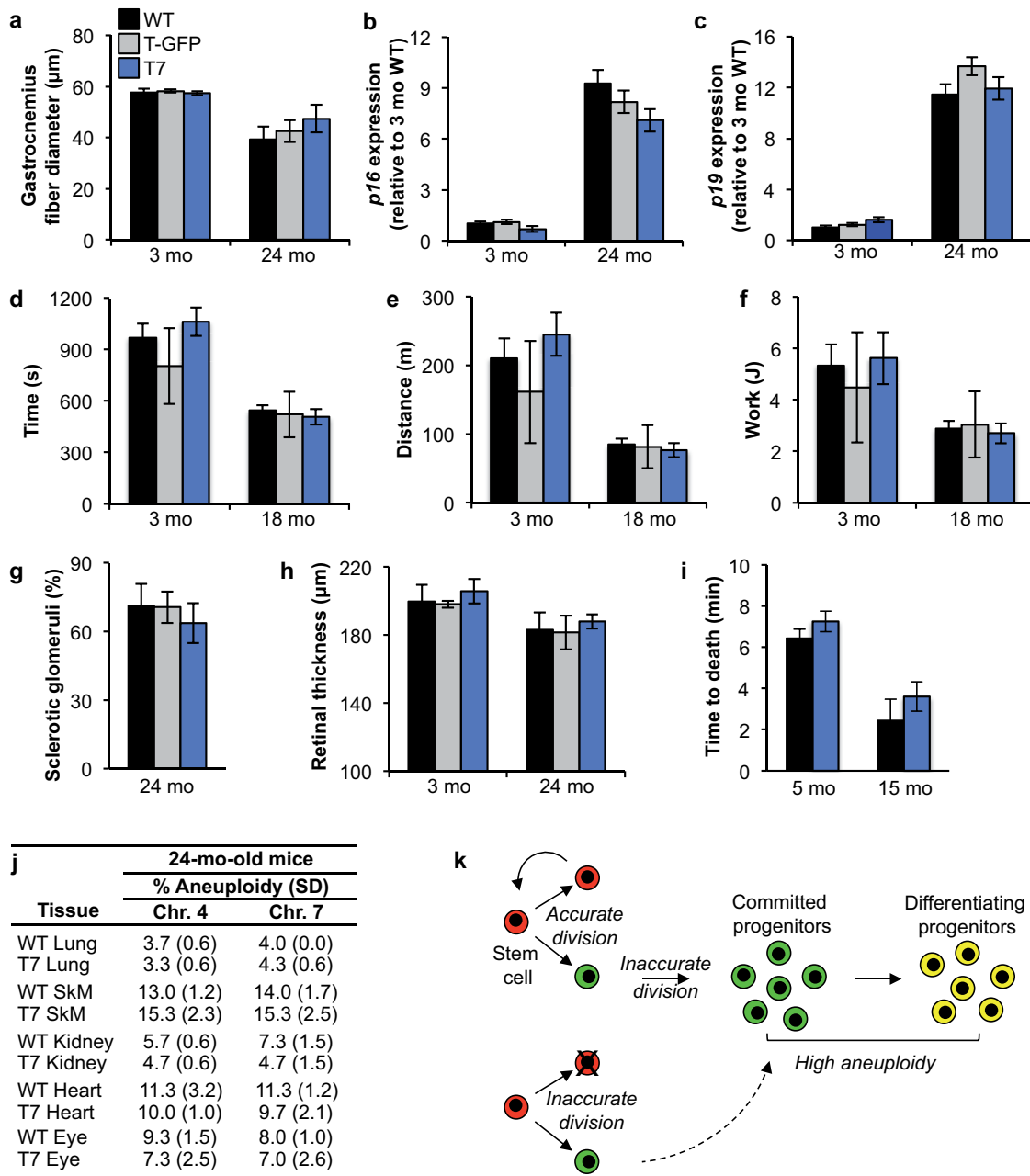
Figure S5 Age-related attenuation of tissue dysfunction requires a threshold level of BubR1 overexpression. **(a)** Gastrocnemius muscle fiber diameter measurements. **(b)** QRT-PCR analysis of $p16^{Ink4a}$ expression in young and old gastrocnemius muscles. **(c)** Same as **(b)** but for $p19^{Arf}$. **(d-f)** Duration of exercise **(d)**, distance travelled **(e)**, and work performed **(f)** in treadmill exercise tests. **(g)** Analysis of glomerulosclerosis. **(h)** Age-related retinal degeneration is not attenuated in T7 mice. **(i)** Cardiac stress tolerance is not improved in T7 animals. For all analyses in **a-i**, n=5 males per genotype per age group, values are means ± SD. **(j)** Interphase FISH analysis on various mouse tissues (n=3 males per genotype per tissue). **(k)** Model for asymmetric aneuploidization of proliferating stems cells and their committed progeny: (top) stem cells segregate their chromosomes with high accuracy, but committed progenitors do not leading to aneuploid differentiated offspring; (bottom) stem cells undergoing inaccurate segregation die, while progenitor daughter cells do not, allowing them to produce aneuploid offspring.
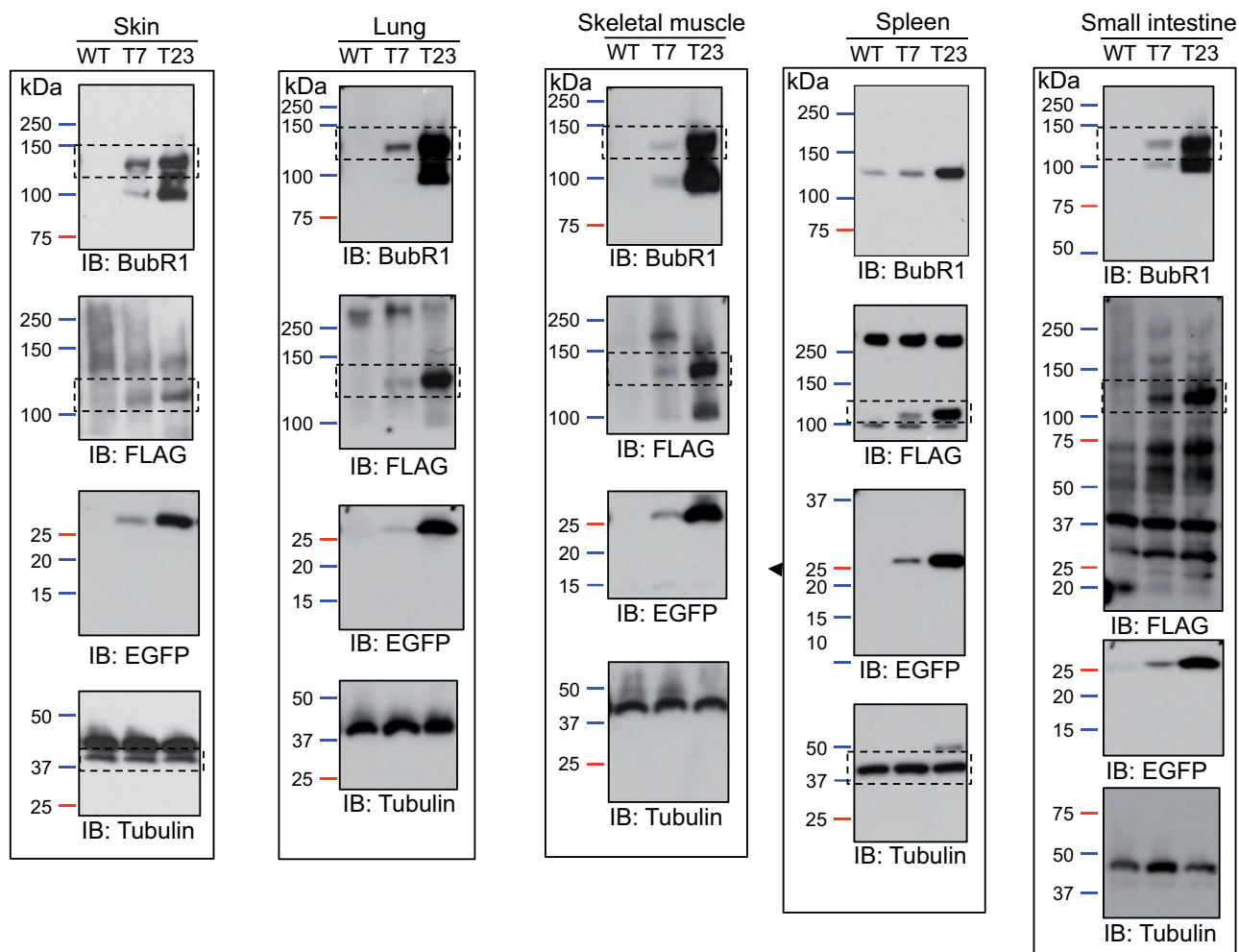
Figure 1b (top panels)

Figure **S6** Full gel scans of key blots in this study
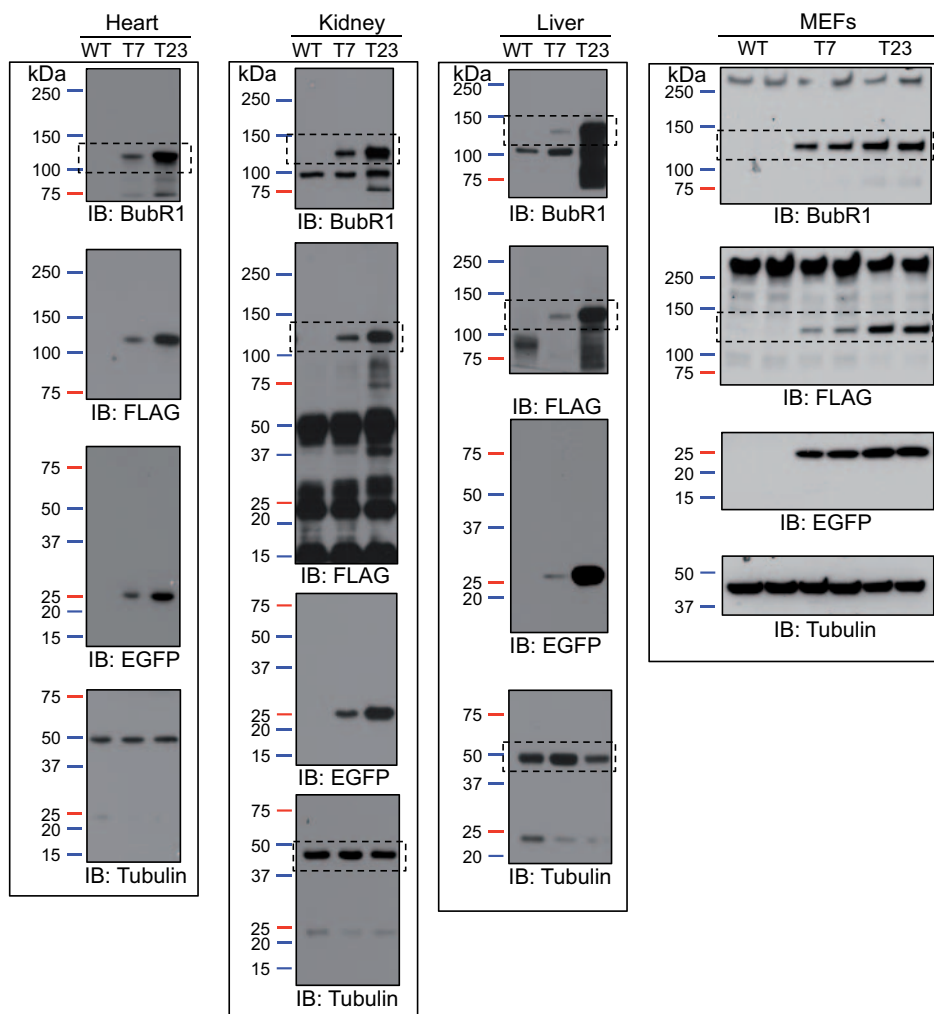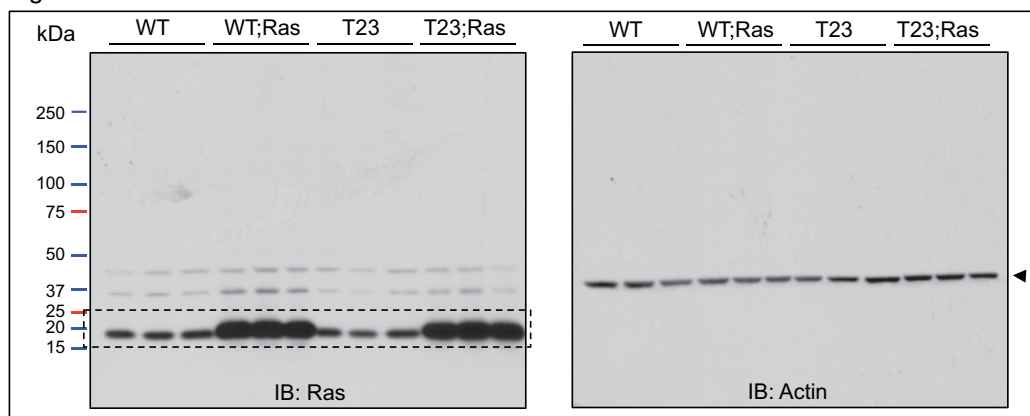
Figure 1b (bottom panels)

Figure 2c

Figure S6 continued